Impact-Free Gaits for Planar Bipeds: Changing Walking Speed and Gait *

Aakash Khandelwal* Nilay Kant** Ranjan Mukherjee***

* Department of Mechanical Engineering, Michigan State University, East Lansing, Michigan (e-mail: khande10@egr.msu.edu) ** Department of Mechanical Engineering, Michigan State University, East Lansing, Michigan (e-mail: kantnila@egr.msu.edu) *** Department of Mechanical Engineering, Michigan State University, East Lansing, Michigan (e-mail: mukherji@egr.msu.edu)

Abstract: The problems of changing the walking speed and stride length of impact-free gaits for point-foot planar bipeds are addressed. The impact-free gaits are designed using an approach developed in prior work. It is shown that the impulse controlled Poincaré map (ICPM) approach can be modified to transition between orbits defining gaits with different walking speeds, and the continuous controller can be changed during the swing phase to transition between gaits that have distinct stride lengths. The effectiveness of the approaches is demonstrated using simulations carried out on a five-link biped.

Keywords: Path Planning and Motion Control, Robotics

NOMENCLATURE

	1 (1)
g	acceleration due to gravity, (m/s ²)
ℓ_j	length of link j , (m)
m_j	mass of link j , (kg)
q	generalized coordinates, $q \triangleq \begin{bmatrix} q_1^T \mid q_2 \end{bmatrix}^T$
$\mathcal{I} \in \mathbb{R}^{n-1}$	impulse of $u_{\mathcal{I}}$
J_i	mass moment of inertia of link j about its
σ_j	
3.5()	center-of-mass, (kgm ²)
M(q)	$n \times n$ symmetric, positive-definite mass
	matrix
V(q)	potential energy of the biped
$u \in R^{n-1}$	control input vector, $u \triangleq [\tau_2 \ \tau_3 \ \cdots \ \tau_n]^T$
u_c	continuous control input, $u_c \equiv u_c(q, \dot{q})$
$u_{\mathcal{I}}$	impulsive control input
$\gamma \in \mathbb{R}^2$	Cartesian coordinates of swing foot, $\gamma \triangleq$
,	$[\gamma_x \ \gamma_u]^T$
0	
$ heta_j$	orientation of link j , measured counter-
	clockwise with respect to the vertical
$ au_{i}$	torque applied on link j by an actuator
3	mounted on link $(j-1)$, (Nm)
$(.)^{-}, (.)^{+}$	variable (.) immediately before and after an
(.) , (.)	
	event where there is a discontinuous jump
	in its value
$(.)^{i}$ $(.)_{0}, (.)_{f}$	variable (.) at the start of the swing phase
$(\cdot)_0$, $(\cdot)_f$	initial and final value of variable or function
(/ 0 / () 1	

1. INTRODUCTION

(.) on distinct gaits

The problem of gait design and stabilization for pointfoot bipeds, which are an important class of underactuated, hybrid systems, has received a lot of attention. Virtual Holonomic Constraints (VHCs), enforced using feedback Maggiore and Consolini (2013); Kant and Mukherjee (2020); Mohammadi et al. (2018), have been successfully used to design biped gaits. The approaches to gait design and stabilization by Grizzle and collaborators Grizzle et al. (2001); Westervelt et al. (2003); Plestan et al. (2003); Westervelt et al. (2018) use Bézier polynomials to paramterize the VHCs. The VHCs are enforced by a nonsmooth controller which drive system trajectories to the constraint manifold within a single swing phase. Asymptotically stable gaits on the constraint manifold are obtained via numerical optimization. Alternative control designs have been presented in Freidovich et al. (2008); Ames et al. (2014).

In Khandelwal et al. (2023), a fundamentally different approach to gait design and stabilization was adopted. A class of VHCs that guaranteed the existence of a family of *impact-free* nominal gaits was proposed. Notably,

- The gait parameters were obtained from solving a set of algebraic equations.
- The walking speed can be chosen independently of the gait parameters, which define the stride length.
- Gait stabilization is achieved independently of the gait design; a continuous controller enforces the VHCs, and intermittent impulsive inputs stabilize the orbit corresponding to a certain walking speed.

This paper extends the work in Khandelwal et al. (2023), and considers the problems of changing the walking speed for a given stride length by changing the impulsive controller, and changing the stride length by changing the continuous controller. Thus, it is shown that it is possible to transition between different orbits on the same constraint manifold, as well as between different constraint manifolds and orbits therein.

 $^{^{\}star}$ This work was supported by the National Science Foundation, under Grant CMMI-2043464.

2. SYSTEM DYNAMICS

2.1 System Description

The *n*-link point-foot planar biped of Khandelwal et al. (2023) is reproduced in Fig.1. A walking gait of the biped comprises a sequence of alternating single-support and double-support phases. For the single-support phase, the *stance leg* of the biped remains in contact with the ground, with the *stance foot* acting as a pivot which does not slide or leave the ground, and permits rotary motion without friction. The single-support phase ends when the *swing leg* comes in contact with the ground, resulting in a double-support phase of infinitesimal duration. This phase involves force interaction between only the swing leg and the ground, and ends with the relabelling of coordinates for interchange of stance and swing legs.

Each leg of the biped is comprised of (n-1)/2 links, with the stance leg links numbered 1 through (n-1)/2 starting from the link in contact with the ground, the torso numbered link (n+1)/2, and the swing leg links numbered (n+3)/2 through n starting from the link in contact with the torso. The link lengths satisfy

$$\ell_{n-j+1} = \ell_j \quad \forall j = 1, 2, \cdots, (n-1)/2$$

We use the generalized coordinates $q \triangleq \begin{bmatrix} q_1^T | q_2 \end{bmatrix}^T$, where $q_1 \in \mathcal{Q}^{n-1}$, $q_2 \in \mathcal{Q}^1$ and $\mathcal{Q}^n \triangleq S^1 \times S^1 \times \cdots \times S^1$, (where S^1 is the unit circle), defined by

$$q = [(\theta_2 - \theta_1) \ (\theta_3 - \theta_2) \ \cdots \ (\theta_n - \theta_{n-1}) | \ \theta_1]^T - \Pi$$
 (1)

where $\Pi \in \mathbb{R}^n$ has elements equal to zero for all entries except for the (n+1)/2 entry, which is equal to π .

2.2 Hybrid Dynamic Model

A complete discussion of the hybrid dynamic model will not be presented here, and is available in Khandelwal et al. (2023). For the purposes of this paper, we note that the hybrid dynamics can be divided into the swing-phase dynamics (during the single-support phase), and the dynamics of foot-ground interaction and coordinate relabelling (during the double support phase).

During the swing phase, the biped represents an n-DOF underactuated system with one passive DOF q_2 , and its

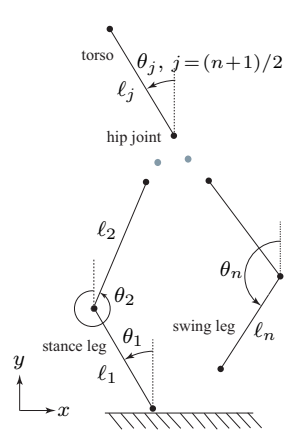


Fig. 1. An *n*-link point-foot planar biped.

equations-of-motion have the form Kant and Mukherjee (2020); Khandelwal et al. (2023):

$$M_{11}(q)\ddot{q}_1 + M_{12}(q)\ddot{q}_2 + h_1(q,\dot{q}) = u$$
 (2a)

$$M_{12}^T(q)\ddot{q}_1 + M_{22}(q)\ddot{q}_2 + h_2(q,\dot{q}) = 0$$
 (2b)

which may be rewritten in the form:

$$\ddot{q}_1 = A(q, \dot{q}) + B(q)u, \quad \ddot{q}_2 = C(q, \dot{q}) + D(q)u$$
 (3)

with the expressions for $A(q, \dot{q}), B(q), C(q, \dot{q}), D(q)$ available in Kant and Mukherjee (2020).

Under the continuous control u_c , the swing phase dynamics has the state-space representation

$$\dot{x} = f(x), \qquad x \triangleq \left[q^T \ \dot{q}^T \right]^T \in \mathcal{Q}^n \times R^n$$
 (4)

Further, any impulsive actuation during the swing phase results in a discontinuous jump in states.

The double support phase comprises impulsive interaction between the swing foot and ground, while the stance foot lifts from the ground without interaction. Following this, there is an instantaneous interchange between the stance and swing legs. Both foot-ground interaction and leg interchange result in discontinuous jumps in the states.

The complete hybrid dynamics of the biped gait can be described by Khandelwal et al. (2023)

$$\mathcal{D}: \begin{cases} \dot{x} = f(x), & x \notin \mathcal{S}, u_{\mathcal{I}} = 0 & \text{1} \\ x^{+} = x^{-} + \Delta x_{\mathcal{I}}, & x^{-} \notin \mathcal{S}, u_{\mathcal{I}} \neq 0 & \text{2} \\ x^{+} = x^{-} + \Delta x_{g}, & x^{-} \in \mathcal{S}_{1} & \text{3} \\ x^{+} = \mathcal{R}(x^{-}), & x^{-} \in \mathcal{S}_{2} & \text{4} \end{cases}$$
 (5)

where

$$S_1 \triangleq \{ x \in \mathcal{Q}^n \times R^n : \gamma_y = 0, \dot{\gamma}_y < 0 \}$$
 (6a)

$$S_2 \triangleq \{ x \in \mathcal{Q}^n \times R^n : \gamma_y = 0, \dot{\gamma} = 0 \}$$
 (6b)

and $S \triangleq S_1 \cup S_2$ is the set of states during the double-support phase. In (5), $\Delta x_{\mathcal{I}}$ and $\Delta x_{\mathbf{g}}$ denote the instantaneous jumps in states due to impulsive actuation $u_{\mathcal{I}}$ and foot-ground impact respectively, and $\mathcal{R}(x)$ is the relabelling map for leg interchange, expressions for which can be found in Khandelwal et al. (2023).

3. IMPACT-FREE GAITS

3.1 Gait Design Considerations

We recall some key aspects of the impact-free gait design from Khandelwal et al. (2023) here. The gaits were designed subject to several boundary conditions. The boundary condition of zero swing-foot velocity at the time of swing-foot touchdown ensured no impact. Additional boundary conditions ensured identical potential and kinetic energies at the beginning and end of the swing phase, and single-step periodicity of the gaits. With the actuated joint trajectories designed to have the form

 $\theta_j = a_j \theta_1 + k_j \pi + \mathcal{G}_j \sin(\mathcal{H}_j \theta_1), \quad j = 2, 3, \dots, n$ (7) where $a_j \in R$, $k_j \in \{0, 1\}$, and $\mathcal{G}_j, \mathcal{H}_j \in R$, $\forall j = 2, 3, \dots, n$, are constants, it was shown (Khandelwal et al., 2023, Appendix) that impact-free gaits satisfying all boundary conditions can always be found for bipeds with

 $n \geq 5$. The parameters are independent of $\dot{\theta}_1^i$, and depend only on the choice of $\theta_1^i \in (0, \pi/2)$. The value of θ_1^i governs the stride length of the gait. The parameters governing the torso motion are chosen to provide sufficient forward moment to enable the biped to take a step.

3.2 VHCs and Orbit Describing Impact-Free Gait

The actuated joint trajectories in (7) are expressed as VHCs in terms of the generalized coordinates q as

$$\rho(q) = q_1 - \Phi(q_2) = 0, \quad \Phi: S^1 \to \mathcal{Q}^{n-1}$$
 (8)

with the choice of generalized coordinates in (1) and parameter choices in (Khandelwal et al., 2023, Appendix) ensuring that the VHCs in (8) are odd, *i.e.*, $\Phi(q_2) = -\Phi(-q_2)$ (Kant and Mukherjee, 2020, Assumption 2), (Khandelwal et al., 2023, Remark 4). The constraint manifold \mathcal{C} corresponding to the VHCs in (8) is

$$C = \left\{ (q, \dot{q}) : q_1 = \Phi(q_2), \dot{q}_1 = \left[\frac{\partial \Phi}{\partial q_2} \right] \dot{q}_2 \right\}$$
 (9)

The VHCs in (8) are regular and C is stabilizable if $M_{12}^T(\partial\Phi/\partial q_2) + M_{22} \neq 0$ (Kant and Mukherjee, 2020, Remark 1), (Khandelwal et al., 2023, Remark 5).

The VHCs in (8) are enforced, and C rendered controlled invariant using the continuous control Kant and Mukherjee (2020)

$$u_c = \left[B - (\partial \Phi/\partial q_2)D\right]^{-1} \left[-A + (\partial^2 \Phi/\partial q_2^2)\dot{q}_2^2 + (\partial \Phi/\partial q_2)C - k_p\rho - k_d\dot{\rho}\right]$$
(10)

where k_p and k_d are positive definite matrices.

Consistent with (8) being satisfied, *i.e.* from substituting (8) in (2b), the swing phase zero dynamics can be expressed as

$$\ddot{q}_2 = \alpha_1(q_2) + \alpha_2(q_2)\dot{q}_2^2 \tag{11}$$

which has an integral of motion of the form $E(q_2, \dot{q}_2) = (1/2)\mathcal{M}(q_2)\dot{q}_2^2 + \mathcal{P}(q_2)$ Kant and Mukherjee (2020), where $\mathcal{P}(q_2)$ has minimum and maximum values \mathcal{P}_{\min} and \mathcal{P}_{\max} . For energy level sets $E(q_2, \dot{q}_2) = c$, a feasible gait is one for which $c > \mathcal{P}_{\max}$, which ensures that the biped is able to complete a step.

The constraint manifold C contains a family of gaits, all of which have the same stride length that depends on the choice of θ_1^i and the gait parameters in (7). Different walking speeds can be achieved by choosing different values of $\dot{\theta}_1^i$, as long as it is greater than some minimum value. Every choice of $\dot{\theta}_1^i$ corresponds to a unique energy level set c^* ; a particular impact-free gait is the hybrid orbit

$$\mathcal{O}^* = \mathcal{C}^* \cup \mathcal{R}^* \tag{12}$$

$$C^* = \{ x \in C : E(q_2, \dot{q}_2) = c^* \}$$
 $c^* > \mathcal{P}_{\text{max}}$ (13a)

$$\mathcal{R}^* = \{x^-, x^+ : x^- \in \mathcal{C}^* \cap \mathcal{S}_2, x^+ = \mathcal{R}(x^-) \in \mathcal{C}^* \}$$
 (13b)

The only jump in states is due to coordinate relabelling.

3.3 Hybrid Orbit Stabilization

The impulse controlled Poincaré map (ICPM) described in Khandelwal et al. (2023) is used to stabilize \mathcal{O}^* . We choose the Poincaré section:

$$\Sigma = \{ x \in \mathcal{Q}^n \times R^n : q_2 = q_2^*, \dot{q}_2 < 0 \}$$
 (14)

where q_2^* is chosen to permit the continuous controller sufficient time to drive system trajectories close to \mathcal{C} . The states on Σ are:

$$z = \begin{bmatrix} q_1^T \ \dot{q}^T \end{bmatrix}^T, \quad z \in \mathcal{Q}^{n-1} \times R^n$$
 (15)

With impulsive inputs \mathcal{I} applied when the system trajectory intersects Σ , the hybrid dynamics of the impulse-controlled system is expressed by the map

$$z(k+1) = \mathbb{P}[z(k), \mathcal{I}(k)] \tag{16}$$

which is obtained numerically and captures the dynamics between successive intersections of the system trajectory with Σ . The intersection of \mathcal{O}^* with Σ is a fixed point $z(k) = z^*$, $\mathcal{I}(k) = 0$ of \mathbb{P} :

$$z^* = \mathbb{P}(z^*, 0) \tag{17}$$

Starting from a system trajectory not on \mathcal{O}^* , intermittent impulsive inputs $\mathcal{I}(k)$ can be used to asymptotically stabilize the fixed point z^* , and consequently the orbit \mathcal{O}^* . The map \mathbb{P} is linearized about $z(k) = z^*$ and $\mathcal{I}(k) = 0$:

$$e(k+1) = Ae(k) + \mathcal{BI}(k), \quad e(k) \triangleq z(k) - z^*$$
 (18)

$$\mathcal{A} \triangleq [\nabla_z \mathbb{P}(z, \mathcal{I})]_{z=z^*, \mathcal{I}=0}$$

$$\mathcal{B} \triangleq [\nabla_{\mathcal{I}} \mathbb{P}(z, \mathcal{I})]_{z=z^*, \mathcal{I}=0}$$
(19)

The matrices $A \in R^{(2n-1)\times(2n-1)}$ and $B \in R^{(2n-1)\times(n-1)}$ are computed numerically. If (A, B) is controllable, the orbit \mathcal{O}^* is rendered asymptotically stable by the discrete feedback:

$$\mathcal{I}(k) = \mathcal{K}e(k) \tag{20}$$

with K chosen such that the eigenvalues of (A + BK) lie inside the unit circle.

The ICPM approach to stabilization of \mathcal{O}^* is depicted in Fig.2. The orbit \mathcal{O}^* (shown in red), intersects Σ at z^* and corresponds to an impact-free gait where the states undergo a single discontinuous jump in states 4 due to coordinate relabelling. A trajectory not on \mathcal{O}^* (shown in black) has additional discontinuous jumps in states 2 on Σ due to application of $\mathcal{I}(k)$, and 3 due to foot-ground impact. As the system trajectory converges to \mathcal{O}^* due to input $\mathcal{I}(k)$, the jumps 2 and 3 converge to zero.

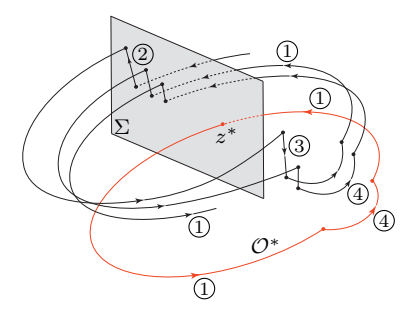


Fig. 2. The ICPM approach to orbital stabilization of an impact-free gait (shown in red). The different components of the hybrid dynamics, namely, ①, ②, ③ and ④ are described by (5).

Remark 1. The high-gain feedback, applied in addition to u_c , is used to realize a continuous-time approximation of impulsive inputs Jafari et al. (2016); Kant and Mukherjee (2020); Khandelwal et al. (2023):

$$u_{\text{hg}} = B^{-1} \left[\frac{1}{\mu} \Lambda (\dot{q}_1^{\text{des}}(k) - \dot{q}_1) - \bar{A} \right]$$
 (21)

where $\dot{q}_1^{\text{des}}(k) = \dot{q}_1(k) + B\mathcal{K}e(k), \ \bar{A} = (1/M_{22})B(q) \times [M_{12}h_2 - (h_1 - u_c)M_{22}], \ \Lambda = \text{diag} \left[\lambda_1 \ \lambda_2 \ \cdots \ \lambda_{n-1}\right], \ \lambda_i > 0, \ i = 1, 2, \cdots, n-1, \ \text{and} \ \mu > 0 \ \text{is a small number. The}$ high-gain feedback remains active as long as $\|\dot{q}_1^{\text{des}}(k) |\dot{q}_1| \geq \epsilon$ where ϵ is a small, positive number.

4. CHANGING WALKING SPEED

We consider the problem of changing the walking speed of the biped while the stride length is kept the same. This is achieved by changing only the value of $\dot{\theta}_1^i$, and consequently c^* , while θ_1^i and the associated gait parameters, i.e. the VHCs, are left unchanged. Thus, the system trajectories during the swing phase evolve on the same constraint manifold \mathcal{C} for both the initial and final gaits; consequently the continuous controller (10) enforcing the VHCs is not altered as it only drives system trajectories to \mathcal{C} . Impulsive inputs are used to guide the system trajectory from one hybrid orbit to another. Let the initial and final orbits be given by $\mathcal{O}_0^* = \mathcal{C}_0^* \cup \mathcal{R}_0^*$ and $\mathcal{O}_f^* = \mathcal{C}_f^* \cup \mathcal{R}_f^*$, where

$$C_0^* = \{ x \in C : E(q_2, \dot{q}_2) = c_0^* \} \qquad c_0^* > \mathcal{P}_{\text{max}}$$
 (22a)

$$\mathcal{R}_0^* = \left\{ x^-, x^+ : x^- \in \mathcal{C}_0^* \cap \mathcal{S}_2, x^+ = \mathcal{R}(x^-) \in \mathcal{C}_0^* \right\}$$
 (22b)

$$C_{\rm f}^* = \{ x \in C : E(q_2, \dot{q}_2) = c_{\rm f}^* \} \qquad c_{\rm f}^* > \mathcal{P}_{\rm max}$$
 (22c)

$$C_{\rm f}^* = \{ x \in \mathcal{C} : E(q_2, \dot{q}_2) = c_{\rm f}^* \} \qquad c_{\rm f}^* > \mathcal{P}_{\rm max}$$

$$\mathcal{R}_{\rm f}^* = \{ x^-, x^+ : x^- \in \mathcal{C}_{\rm f}^* \cap \mathcal{S}_2, x^+ = \mathcal{R}(x^-) \in \mathcal{C}_{\rm f}^* \}$$
(22c)

In transitioning from \mathcal{O}_0^* to \mathcal{O}_f^* , the value of $\dot{\theta}_1^i$ (consequently, c^*) is changed gradually over a finite number of steps, as in Khandelwal et al. (2024), by choosing

$$\dot{\theta}_{1}^{i} = \begin{cases} \dot{\theta}_{10}^{i} & k \leq k_{0} \\ F(k) & k_{0} < k < k_{f} \\ \dot{\theta}_{1f}^{i} & k \geq k_{f} \end{cases}, \quad F(k_{0}) = \dot{\theta}_{10}^{i}, F(k_{f}) = \dot{\theta}_{1f}^{i}$$

where F(k) is a monotonic function. For every intersection of the system trajectory with Σ when $k \in (k_0, k_{\rm f})$, the fixed point $z^* \equiv z^*(k)$ must be recomputed. F(k) must be chosen to ensure that every intersection of the system trajectory with Σ lies within the domain of linearization of $z^*(k)$, and the impulsive torques demanded are reasonable. For $k \leq k_0$, $z^*(k) = z_0^*$, and for $k \geq k_f$, $z^*(k) = z_f^*$. The ICPM approach of (18) and (19) is rewritten as

$$e(k+1) = \mathcal{A}(k)e(k) + \mathcal{B}(k)\mathcal{I}(k), \quad e(k) \triangleq z(k) - z^*(k)$$
(24)

$$\mathcal{A}(k) \triangleq \left[\nabla_z \mathbb{P}(z, \mathcal{I})\right]_{z=z^*(k), \mathcal{I}=0}$$

$$\mathcal{B}(k) \triangleq \left[\nabla_{\mathcal{I}} \mathbb{P}(z, \mathcal{I})\right]_{z=z^*(k), \mathcal{I}=0}$$
(25)

It must be ensured that the pair [A(k), B(k)] is controllable $\forall k$, and the gain matrix \mathcal{K} in (20) must be recomputed for every $k \in \{k_0, ..., k_f\}$.

5. CHANGING STRIDE LENGTH

A change in the stride length of the biped requires a change in the value of θ_1^i and associated gait parameters, resulting in distinct VHCs $\Phi_0 \equiv \Phi_0(q_2)$ and $\Phi_f \equiv \Phi_f(q_2)$ for the initial and final gaits, and associated constraint manifolds:

$$C_0 = \left\{ (q, \dot{q}) : q_1 = \Phi_0(q_2), \dot{q}_1 = \left[\frac{\partial \Phi_0}{\partial q_2} \right] \dot{q}_2 \right\}$$
 (26)

$$C_{\rm f} = \left\{ (q, \dot{q}) : q_1 = \Phi_{\rm f}(q_2), \dot{q}_1 = \left[\frac{\partial \Phi_{\rm f}}{\partial q_2} \right] \dot{q}_2 \right\} \tag{27}$$

each of which comprise families of impact-free gaits with different stride lengths. The VHCs Φ_0 and Φ_f are enforced by the continuous controllers:

$$u_{c0} = [B - (\partial \Phi_0 / \partial q_2)D]^{-1} [-A + (\partial^2 \Phi_0 / \partial q_2^2) \dot{q}_2^2 + (\partial \Phi_0 / \partial q_2)C - k_p \rho_0 - k_d \dot{\rho}_0]$$
(28)
$$u_{cf} = [B - (\partial \Phi_f / \partial q_2)D]^{-1} [-A + (\partial^2 \Phi_f / \partial q_2^2) \dot{q}_2^2 + (\partial \Phi_f / \partial q_2)C - k_p \rho_f - k_d \dot{\rho}_f]$$
(29)

We wish to transition from a gait on C_0 to one on C_f . To do this, the continuous controller in (28) enforcing the initial VHCs Φ_0 is changed to the one in (29) to enforce the new VHCs Φ_f at step k_s when the switch is desired. While the change from u_{c0} to u_{cf} may be performed at any point during the swing phase of step k_s , we choose to do this when the system trajectory passes through $q_2 = 0$ since this represents the intersection of the initial and final VHCs, which are odd functions, i.e.

$$\Phi_0(0) = \Phi_f(0) = 0 \tag{30}$$

(29)

Once the continuous controller has been changed, the ICPM approach described in section 3.3 can be used to stabilize the orbit corresponding to the desired walking speed on \mathcal{C}_{f} .

6. CASE STUDY: FIVE-DOF BIPED

The approaches developed in sections 4 and 5 will be applied to the five-link biped in Khandelwal et al. (2023), whose kinematic and dynamic parameters are reproduced in Table 1. The expressions for the matrices in (2) can be deduced from Jafari et al. (2013).

An impact-free gait for this biped is described by the actuated joint trajectories

$$\theta_j = a_j \theta_1 + k_j \pi + \mathcal{G}_j \sin(\mathcal{H}_j \theta_1), \quad j = 2, 3, 4, 5 \tag{31}$$

For a gait described by (31) and the choice $\theta_1^i = \pi/20$, a set of feasible gait parameters are listed in Table 2 Khandelwal et al. (2023). This gait has a stride length of 0.5371 m.

Using (31) and the parameters in Table 2, the VHCs in (8) can be expressed as:

$$\rho(q) = q_1 - \Phi(q_2) = 0, \quad \Phi : S^1 \to \mathcal{Q}^4$$

$$\Phi = \begin{bmatrix} -0.3500q_2 + 0.1023\sin(20q_2) \\ -0.6500q_2 - 0.2773\sin(20q_2) \\ -0.6500q_2 + 0.2123\sin(20q_2) \\ -1.1761q_2 - 0.0373\sin(20q_2) - 0.1706\sin(25.5q_2) \end{bmatrix}$$
(32)

Table 1. Kinematic and dynamic parameters of five-link biped

j	ℓ_j (m)	d_j (m)	m_j (kg)	$J_j \text{ (kg m}^2\text{)}$
1, 5	0.5000	0.2500	0.4000	0.0083
2, 4	0.5500	0.2750	0.4500	0.0113
3 (torso)	0.6000	0.4200	0.5500	0.0165

Table 2. Gait parameters for $\theta_1^i = \pi/20$

j	a_{j}	k_j	\mathcal{G}_{j}	\mathcal{H}_{j}
2	0.6500	0	0.1023	20.0
3 (torso)	0.0000	0	-0.1750	20.0
4	-0.6500	1	0.0373	20.0
5	-1.8261	1	-0.1706	25.5

which are enforced by the continuous controller in (10) with gain matrices

$$k_p = 450 I_4, \quad k_d = 40 I_4$$
 (33)

where $I_n \in R^{n \times n}$ is the identity matrix. In Khandelwal et al. (2023), the orbit defined by $\dot{\theta}_1^i = -1.0891$ rad/s, which corresponds to a walking speed of 1.1554 m/s was stabilized. This orbit is treated as the initial gait for the simulations in the subsequent two sections.

6.1 Changing Walking Speed

For the constraint manifold defined by the VHCs in (32), we wish to transition from the orbit \mathcal{O}_0^* defined by $\dot{\theta}_{10}^i = -1.0891 \text{ rad/s}$ to $\mathcal{O}_{\rm f}^*$ defined by $\dot{\theta}_{1\rm f}^i = -0.8713 \text{ rad/s}$. This corresponds to a change in walking speed from 1.1554 to 0.7218 m/s. As described in (23), the value of $\dot{\theta}_1^i$ is changed following the rule:

$$\dot{\theta}_1^i = \begin{cases} -1.0891 & k \le 2\\ -1.0891 + 0.0311(k-2) & 2 < k < 9\\ -0.8713 & k \ge 9 \end{cases}$$
 (34)

We choose the Poincaré section:

$$\Sigma = \{ x \in \mathcal{Q}^5 \times R^5 : q_2 = \pi/40, \dot{q}_2 < 0 \}$$
 (35)

on which to apply impulsive inputs. The states on Σ are $z, z \in \mathcal{Q}^4 \times R^5$, as defined in (15). For $k \in \{2, \dots, 9\}$, the fixed point $z^* \equiv z^*(k)$ is recomputed for every $\dot{\theta}_1^i$. For $k \leq 2$, $z^*(k) = z_0^*$, the intersection of \mathcal{O}_0^* with Σ , and for $k \geq 9$, $z^*(k) = z_{\mathrm{f}}^*$, the intersection of $\mathcal{O}_{\mathrm{f}}^*$ with Σ . The linearized matrices $\mathcal{A}(k) \in R^{9 \times 9}$ and $\mathcal{B}(k) \in R^{9 \times 4}$ are computed numerically for each $z^*(k)$. Every pair $[\mathcal{A}(k), \mathcal{B}(k)]$ is found to be controllable, and the gain matrices \mathcal{K} obtained using LQR with the weighting matrices

$$Q = \text{blockdiag}[I_4 \ 1.5I_5], \quad R = 2.5I_4$$
 (36)

The simulation results are shown in Fig. 3 for 16 steps, which corresponds to a duration of approx. 9.80 s. The impulsive inputs are realized using the high-gain feedback in (21), with the choices:

$$\Lambda = I_4, \quad \mu = 0.0025, \quad \epsilon = 0.0001$$
 (37)

The components of $\rho(q)$ plotted in Fig. 3(a)-(d) demonstrate convergence of the system trajectories to \mathcal{C} , with the jumps in ρ corresponding to the instants of application of impulsive inputs. The joint torques τ_j are plotted in Fig. 3(e)-(h), with the impulsive torques shown in red. Clearly, the values of u_c are large after $u_{\rm hg}$ terminates. It can be seen that impulsive inputs are not applied for k>14 as the system trajectories are sufficiently close to $\mathcal{O}_{\rm f}^*$. The phase the passive joint is shown in Fig. 3(i) for t<4 s and Fig. 3(j) for $t\geq 4$ s.

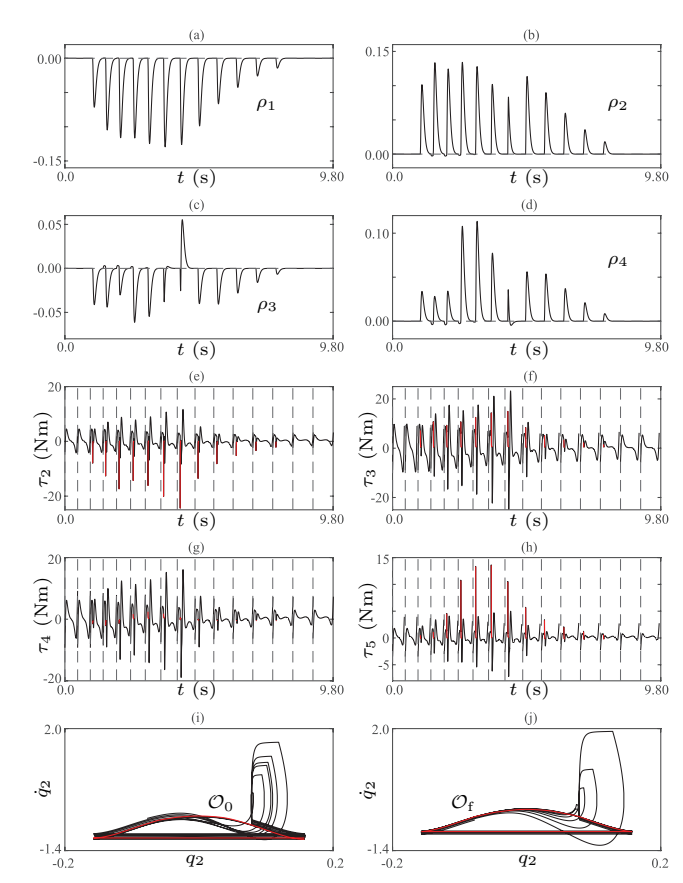


Fig. 3. Changing walking speed using the ICPM approach: (a)-(d) show the components of $\rho(q)$, (e)-(h) show the joint torques $\tau_j, j=2,3,4,5$, with impulsive torques shown in red, (i) shows the phase portrait of the passive coordinate for t<4 s, with the initial orbit shown in red, and (j) for $t\geq 4$ s, with the final orbit shown in red.

Table 3. Gait parameters for $\theta_1^i = \pi/16$

j	a_{j}	k_{j}	\mathcal{G}_{j}	\mathcal{H}_j
2	0.6500	0	0.1277	16.0
3 (torso)	0.0000	0	-0.1750	16.0
4	-0.6500	1	0.0465	16.0
5	-1.8261	1	-0.2133	20.4

6.2 Changing Stride Length

We demonstrate transition from a gait with $\theta_1^i = \pi/20$ and parameters in Table 2 to one with $\theta_1^i = \pi/16$ and parameters in Table 3. The initial gait is defined by the VHCs Φ_0 , which are identical to those in (32). The initial orbit on C_0 corresponds to $\dot{\theta}_1^i = -1.0891$ rad/s.

The final gait has a stride length of $0.6702~\mathrm{m},$ and is defined by the VHCs

$$\rho_{\rm f}(q) = q_1 - \Phi_{\rm f}(q_2) = 0, \quad \Phi_{\rm f}: S^1 \to \mathcal{Q}^4$$

$$\Phi_{\rm f} = \begin{bmatrix} -0.3500q_2 + 0.1277\sin(16q_2) \\ -0.6500q_2 - 0.3027\sin(16q_2) \\ -0.6500q_2 + 0.2215\sin(16q_2) \\ -1.1761q_2 - 0.0465\sin(16q_2) - 0.2133\sin(20.4q_2) \end{bmatrix}$$
(38)

The desired orbit on C_f that we wish to stabilize is the one for which $\dot{\theta}_1^i = -1.5453$ rad/s, which results in the

same walking speed, 1.1554 m/s, as the initial orbit on C_0 . The continuous controller is changed from (28) to (29) when $q_2 = 0$ on step 2; the gains k_p and k_d are given in (33). With the same Poincaré section as in (35), the intersection of the final orbit (on C_f) with Σ represents the fixed point to be stabilized by the ICPM approach. Again, the pair $(\mathcal{A}, \mathcal{B})$, obtained by linearization about the new fixed point, is controllable, and the gain matrix \mathcal{K} obtained using LQR with the weighting matrices in (36).

The simulation results are shown in Fig. 4 for 10 steps, a duration of approx. 5.57 s. The impulsive inputs are realized using the high-gain feedback in (21) with parameter choices (37). The instant the VHCs are changed from Φ_0 to Φ_f is $t\approx 0.70$ s. Figure 4(a)-(d) shows the components of $\rho_0(q)$ for t<0.70 s and $\rho_f(q)$ for $t\geq0.70$ s. For $t\geq0.70$ s, the controller u_{cf} drives system trajectories to C_f . The joint torques τ_j are plotted in Fig. 4(e)-(h), with the impulsive torques shown in red. Impulsive torques are required for k=3 through k=6 to drive system trajectories sufficiently close to the desired orbit on C_f . The phase the passive joint is shown in Fig. 4(i) for t<2 s and Fig. 4(j) for $t\geq2$ s.

7. CONCLUSION

The problems of changing the walking speed of an impact-free gait with a given stride length, and of transitioning between impact-free gaits with distinct stride lengths are addressed. The first problem was solved by the use of a variation of the impulse controlled Poincaré map approach to transition between distinct orbits on the same constraint manifold. The solution to the second problem involved switching the continuous controller when the constraint manifolds describing the distinct stride lengths intersected. The efficacy of the proposed approaches is illustrated by simulations of a five-link biped. Future work will focus on the robustness of the gait design.

REFERENCES

Ames, A.D., Galloway, K., Sreenath, K., and Grizzle, J.W. (2014). Rapidly Exponentially Stabilizing Control Lyapunov Functions and Hybrid Zero Dynamics. *IEEE Transactions on Automatic Control*, 59(4), 876–891.

Freidovich, L.B., Shiriaev, A.S., and Manchester, I.R. (2008). Stability Analysis and Control Design for an Underactuated Walking Robot via Computation of a Transverse Linearization. *IFAC Proceedings Volumes*, 41(2), 10166–10171.

Grizzle, J., Abba, G., and Plestan, F. (2001). Asymptotically stable walking for biped robots: Analysis via systems with impulse effects. *IEEE Transactions on Automatic Control*, 46(1), 51–64.

Jafari, R., Flynn, L.L., Hellum, A., and Mukherjee, R. (2013). Energy-Conserving Gaits for Point-Foot Planar Bipeds: A Five-DOF Case Study. In ASME Dynamic Systems and Control Conference. Palo Alto, CA.

Jafari, R., Mathis, F.B., Mukherjee, R., and Khalil, H. (2016). Enlarging the region of attraction of equilibria of underactuated systems using impulsive inputs. *IEEE Trans on Control Systems Technology*, 24(1), 334–340.

Kant, N. and Mukherjee, R. (2020). Orbital Stabilization of Underactuated Systems using Virtual Holonomic

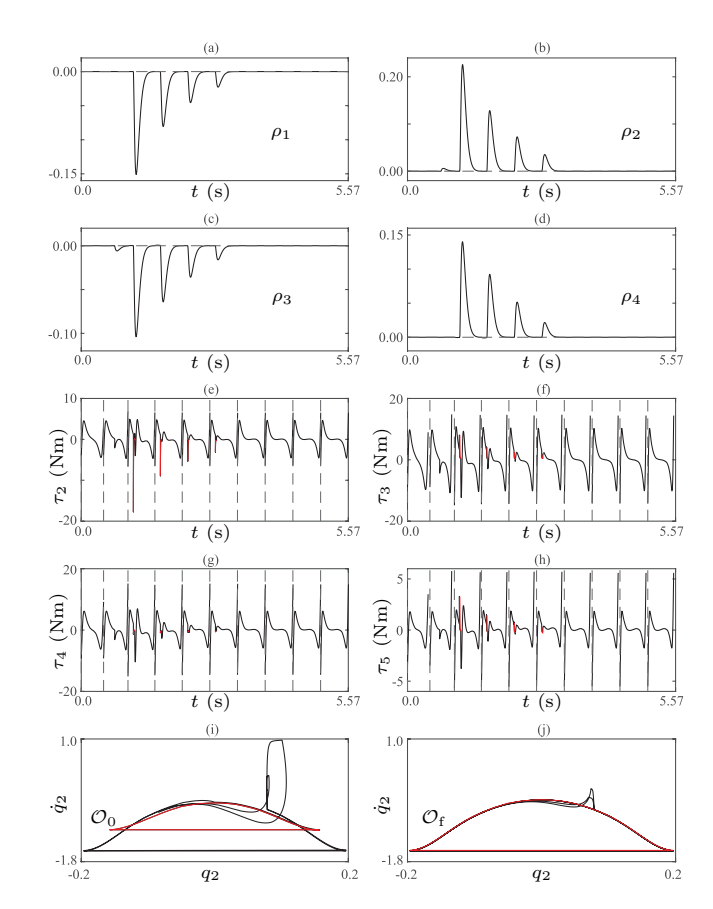


Fig. 4. Changing stride length: (a)-(d) show the components of $\rho_0(q)$ and $\rho_f(q)$, (e)-(h) show the joint torques $\tau_j, j=2,3,4,5$, with impulsive torques shown in red, (i) shows the phase portrait of the passive coordinate for t<2 s, with the initial orbit shown in red, and (j) for $t\geq 2$ s, with the final orbit shown in red.

Constraints and Impulse Controlled Poincaré Maps. Systems & Control Letters, 146, 104813.

Khandelwal, A., Kant, N., and Mukherjee, R. (2023). Design of Impact-Free Gaits for Planar Bipeds and Their Stabilization Using Impulsive Control. *IEEE Robotics and Automation Letters*, 8(11), 7242–7248.

Khandelwal, A., Kant, N., and Mukherjee, R. (2024). Maneuvering a Stick in Three-Dimensional Space Using Impulsive Forces. In *Advances in Nonlinear Dynamics*, *Volume II*, 199–209. Springer Nature Switzerland.

Maggiore, M. and Consolini, L. (2013). Virtual Holonomic Constraints for Euler–Lagrange Systems. *IEEE Transactions on Automatic Control*, 58(4), 1001–1008.

Mohammadi, A., Maggiore, M., and Consolini, L. (2018). Dynamic virtual holonomic constraints for stabilization of closed orbits in underactuated mechanical systems. *Automatica*, 94, 112–124.

Plestan, F., Grizzle, J.W., Westervelt, E.R., and Abba, G. (2003). Stable walking of a 7-dof biped robot. *IEEE Trans on Robotics and Automation*, 19(4), 653–668.

Westervelt, E., Grizzle, J., and Koditschek, D. (2003). Hybrid zero dynamics of planar biped walkers. *IEEE Transactions on Automatic Control*, 48(1), 42–56.

Westervelt, E.R., Grizzle, J.W., Chevallereau, C., Choi, J.H., and Morris, B. (2018). Feedback Control of Dynamic Bipedal Robot Locomotion. CRC Press, Boca Raton.